The C-Terminus of Glutathione *S*-Transferase A1-1 Is Required for Entropically-Driven Ligand Binding[†]

Brenda S. Nieslanik, Catherine Ibarra, and William M. Atkins*

Department of Medicinal Chemistry, Box 357610, University of Washington, Seattle, Washington 98195

Received August 9, 2000; Revised Manuscript Received January 26, 2001

ABSTRACT: Binding of a hydrophobic glutathione product conjugate to rGST A1-1 proceeds via a two-step mechanism, including rapid ligand docking, followed by a slow isomerization to the final [GST·ligand] complex, which involves the localization of the flexible C-terminal helix. These kinetically resolved steps have been observed previously by stopped-flow fluorescence with the wild-type rGST A1-1, which contains a native Trp-21 approximately 20 Å from the ligand binding site at the intrasubunit domain−domain interface. To confirm this binding mechanism, as well as elucidate the effects of truncation of the C-terminus, we have further characterized the binding and dissociation of the glutathione−ethacrynic acid product conjugate (GS-EA) to wild-type, F222W:W21F, and Δ209−222 rGST A1-1 and wild-type hGST A1-1. Although modest kinetic differences were observed between the hGST A1-1 and rGST A1-1, stopped-flow binding studies with GS-EA verified that the two-step mechanism of ligand binding is not unique to the GST A1-1 isoform from rat. An F222W:W21F rGST A1-1 double mutant provides a direct fluorescence probe of changes in the environment of the C-terminal residue. The observation of two relaxation times during ligand binding and dissociation to F222W:W21F suggests that the C-terminus has an intermediate conformation following ligand docking, which is distinct from its conformation in the apoenzyme or localized helical state. For the wild-type, Δ209−222, and F222W:W21F proteins, variable-temperature stopped-flow experiments were performed and activation parameters calculated for the individual steps of the binding reaction. Activation parameters for the binding reaction coordinate illustrate that the C-terminus provides a significant entropic contribution to ligand binding, which is completely realized within the initial docking step of the binding mechanism. In contrast, the slow isomerization step is enthalpically driven. The partitioning of entropic and enthalpic components of binding energy was confirmed by isothermal titration calorimetry with wild-type and Δ209−222 rGST A1-1.

The glutathione *S*-transferases (GSTs)[1] are a family of dimeric detoxication enzymes, which catalyze the conjugation of glutathione (GSH) to a variety of endogenous and exogenous electrophiles. The mammalian cytosolic GSTs are separated into seven gene classes based on crystal structure and substrate specificity: alpha (A), pi (P), mu (M), theta (T), kappa (K), sigma (S), and zeta (Z) (*1*−*5*). X-ray crystallographic and site-directed mutagenesis studies illustrate that each GST contains a conserved tyrosine or serine residue which hydrogen bonds to and effectively deprotonates GSH to the nucleophilic thiolate (GS^-) (*6*−*10*). Because the thiolate anion is a more reactive nucleophile than the protonated thiol, the catalytic advantage is obvious (*11*). Crystal structures indicate that each GST has the same basic protein fold, which consists of two domains; one domain provides the binding site for GSH (G-site), and the second contributes to binding of the hydrophobic ligand (H-site) (*12*). Although the G-site is highly homologous in all of the GSTs, there is a great deal of variability in the H-site, which confers the differing substrate selectivity and catalytic properties for each gene class.

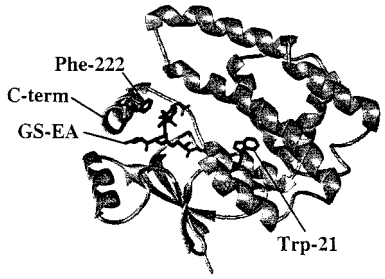

FIGURE 1: Ribbon representation of the hGST A1-1 monomer, illustrating the positions of Trp-21 and Phe-220, is adapted from PDB file 1GSE (*13*). The Trp-21 and Phe-222 residues were mutated to a phenylalanine and tryptophan, respectively, to produce the F222W:W21F double mutant, which provides a direct fluorescence probe of changes in the environment of the C-terminal residue.

A unique structural feature of GST A1-1 is the C-terminal helix (residues 208−222), which is localized over the enzyme active site in the presence of an H-site ligand (Figure 1) (*13*,

[†] This work was supported by an ACS Fellowship Award from Abbott Laboratories, a National Research Service Award (1F31GM20088-01) from the National Institutes of Health, and the Department of Medicinal Chemistry at the University of Washington.

* Corresponding author. Phone: (206) 685-0379, FAX: (206) 685-3252, E-mail: winky@u.washington.edu.

[1] Abbreviations: CDNB, 1-chloro-2,4-dinitrobenzene; EA, ethacrynic acid; F222W:W21F, the rGST A1-1 variant with a tryptophan at residue 222 and a phenylalanine at residue 21; GS-EA, the Michael adduct of ethacrynic acid and glutathione; GSH, glutathione; GS-EA, the synthesized glutathione−ethacrynic acid product conjugate; GST, glutathione *S*-transferase; hGST A1-1, GST A1-1 from human; ITC, isothermal titration calorimetry; WT rGST A1-1, wild-type GST A1-1 from rat; Δ209−222, the rGST A1-1 C-terminal truncation mutant.

10.1021/bi001869x CCC: $20.00
Published on Web 03/01/2001

Scheme 1

$$\text{Ligand + GST} \underset{k_{-1}}{\overset{k_1}{\rightleftharpoons}} [\text{GST•Ligand}]_{dis} \underset{k_{-2}}{\overset{k_2}{\rightleftharpoons}} [\text{GST•Ligand}]_{ord}$$

14). Interestingly, however, in crystal structures of the apo- or G-site-bound GST A1-1, the C-terminal residues are crystallographically 'invisible' (*13*−*15*). Due to low levels of electron density in the expected position of the helix in the apoenzyme crystal structure, as well as the primary sequence of the C-terminus which suggests that it will not fold independently of the rest of the protein, the C-terminal residues most likely comprise a heterogeneous ensemble of dynamic helices, rather than a completely disordered coil in this crystallographically unobservable form (*13*, *16*). Consequently, this C-terminal structural change, that occurs upon ligand binding, can be best described as a transition between a dynamic and localized helix.

Our previous studies illustrate that ligand binding to rGST A1-1 proceeds via a two-step mechanism, which includes ligand 'docking', followed by an isomerization between an intermediate precomplex, $[GST•ligand]_{dis}$, and a final equilibrium complex, $[GST•ligand]_{ord}$ (Scheme 1) (*17*, *18*). In Scheme 1, the subscripts 'dis' and 'ord' refer to a dynamic or disordered C-terminus and the crystallographically visible, localized helix, respectively.

Stopped-flow fluorescence results clearly demonstrate the involvement of the C-terminus in the isomerization phase of the mechanism (*17*, *18*). In ligand binding studies with wild-type (WT) rGST A1-1, two relaxation times were observed spectroscopically, while a single relaxation was visible during ligand binding to a C-terminal truncation mutant, Δ209−222, characteristic of a single-step binding mechanism (*17*). These studies utilized the native Trp-21 as the fluorescent reporter in rGST A1-1, which lies outside of the C-terminus, approximately 20 Å from the active site at the interface between domains I and II within each subunit (Figure 1) (*16*, *19*). Therefore, global changes in protein conformation are apparently induced by both ligand docking (k_1) and isomerization (k_2). The catalytic relevance of this isomerization step, in particular, has been illustrated in steady-state turnover studies, as product release is rate-limiting for several GST/substrate combinations (*20*). Therefore, this conformational change is a critical feature of GST A1-1 function.

To extend this binding model, the kinetics of binding and dissociation were monitored in hGST A1-1, the GST A1-1 isoform from human. Because the structurally homologous rat and human GST A1-1 isoforms contain some amino acid differences within the C-terminus, it is useful to compare their ligand-dependent C-terminal dynamics. As described, however, ligand binding to both hGST A1-1 and rGST A1-1 utilizes the native Trp-21 as a probe of global conformational changes which occur upon ligand binding (*16*, *19*). Because a fluorescence probe incorporated directly into the C-terminus may reveal localized structural changes, ligand binding and dissociation were also monitored in F222W:W21F rGST A1-1, where a tryptophan substituted at the C-terminal residue provides a direct probe of the dynamics of the C-terminus (Figure 1).

Although these kinetic studies have yielded very important mechanistic information about ligand binding and dissociation to GST A1-1, they provide little insight into the forces which drive ligand binding and the corresponding localization of the helix. Equilibrium dissociation constants of WT and Δ209−222 for the glutathione−ethacrynic acid product conjugate (GS-EA) are similar (2.69 versus 6.38 μM, respectively), suggesting that ligand itself does not induce helix stability (*17*). Additionally, in crystal structures of hGST A1-1 with various H-site ligands bound, there is minimal contact between the ligand and the localized helix (*13*, *14*). Therefore, apparently, protein−protein interactions between the C-terminal and other active site residues are more important in stabilization of the closed helical conformation than protein−ligand interactions (*21*). To expand our understanding of the role of the dynamic C-terminus in GST A1-1 catalysis, we have also elucidated the thermodynamic forces that drive ligand binding and the corresponding C-terminal transition in GST A1-1.

As described herein, our ligand binding studies with hGST A1-1 demonstrate a similar concentration dependence of the observed relaxation times to WT rGST A1-1, confirming that the proposed two-step binding mechanism in WT rGST A1-1 is not specific to the rat isoform. Two relaxation times also best described ligand binding and dissociation to F222W:W21F rGST A1-1, which contains a fluorescent probe at the C-terminal residue. These results illustrate that the C-terminal residues have a different conformation in the intermediate precomplex than in the apoenzyme or localized, well-packed helical state. In fact, that binding and dissociation rates were nearly identical to those found in WT rGST A1-1, suggests that global changes in protein conformation are coupled to the localized structural changes at the C-terminus. However, our thermodynamic studies provide the most striking results from these experiments; the C-terminus is required for the entropically-driven ligand binding in GST A1-1, which is completely limited to the docking step of the binding mechanism. In contrast, the isomerization step is enthalpically driven.

MATERIALS AND METHODS

Chemicals and Instrumentation. GSH, EA, CDNB, and MES were obtained from Sigma (St. Louis, MO). GS-EA was synthesized and its purity analyzed as described (*17*, *22*). Stopped-flow binding and dissociation experiments were performed with a BioLogic SFM/QFM fluorimeter. Isothermal titration calorimetry was performed with a CSC 4200 titration calorimeter (Calorimetry Sciences Corporation, Provo, UT).

Protein Expression, Purification, and Activity. The expression and purification of WT rGST A1-1 and Δ209−222 have been described previously (*17*, *23*). The F222W:W21F mutant was constructed by PCR-based amplification of a fragment spanning the *Bgl*II and *Sal*I restriction sites contained in the linearized pKKGTB34-W21F plasmid. The pKKGTB34 plasmid has been described previously (*24*). The sequence of the oligonucleotide primer encoding the F222W mutation was 5′-GCTGCAGGGGCCGTCGACCTACCACT-TGAAAACCTTCCT-3′ and spanned the *Sal*I site. The final PCR product was digested with *Bgl*II and *Sal*I and subcloned into pKKGTB34-W21F that was digested with similar enzymes. Conditions for the PCR reactions were 10 mM $(NH_4)_2SO_4$, 20 mM Tris (pH 8.3), 3 mM $MgSO_4$, 200 μM

each dNTP, 0.1% Triton X-100, 10 mg of linearized template, and 1 unit of Vent DNA polymerase (New England Biolabs). The cycle profiles were 94 °C for 1 min, 65 °C for 1 min, and 72 °C for 1 min for 25 cycles, followed by 10 min at 72 °C. The F222W:W21F mutant was validated by DNA sequencing. The hGST A1-1 clone was a kind gift from Dr. Kenneth Tew, Fox Chase Cancer Center, Philadelphia, PA. Enzymatic activity for each protein was determined using the substrates CDNB and EA (*25*).

GST Binding and Dissociation Kinetics. Conditions for binding and dissociation experiments were similar to those described previously (*17*, *18*). Binding rates were measured by the decrease in protein fluorescence after rapidly mixing an equal volume of 2 μM GST and 20 μM−1 mM GS-EA from 10 to 40 °C. The observed rates, k_{obs}, were determined by fitting the raw data to a double (eq 1) or single (eq 2) exponential decay equation:

$$f(x) = a_1 \exp^{(-k_{obs1}t)} + a_2 \exp^{(-k_{obs2}t)} + C \quad (1)$$

$$f(x) = a_1 \exp^{(-k_{obs}t)} + C \quad (2)$$

where a_1 and a_2 represent the amplitudes of two exponential decays with rate constants k_{obs1} and k_{obs2}, t is time, and C represents the offset.

When two rates were observed, the rapid association and dissociation rates, k_1 and $k_{-1(calc)}$, were determined by fitting a plot of k_{obs1} versus GS-EA concentration to a linear eq 3:

$$k_{obs1} = k_{-1(calc)} + k_1[\text{GS-EA}] \quad (3)$$

The association and dissociation rates of the slower step of the reaction, k_2 and $k_{-2(calc)}$, were determined by fitting a plot of k_{obs2} versus GS-EA concentration to the hyperbolic eq 4:

$$k_{obs2} = k_{-2(calc)} + \frac{k_2}{1 + \frac{K_1}{[\text{GS-EA}]}} \quad (4)$$

Under conditions when a single rate was observed, plots of the observed rate, k_{obs}, versus GS-EA concentration also fit best to a hyperbolic curve (eq 5):

$$k_{obs} = k_{-2(calc)} + \frac{k_2[\text{GS-EA}]}{[\text{GS-EA}] + K_1} \quad (5)$$

Product dissociation from the [GST·GS-EA] complex was directly monitored by the increase in fluorescence intensity after rapidly mixing a solution of 2 μM GST and 20−100 μM GS-EA with 5 mM of the trapping agent, GS-sulfonate (GSO_3^-), which causes no intrinsic protein fluorescence change upon binding (*17*). The dissociation constants, $k_{-1(exp)}$ and $k_{-2(exp)}$, were obtained directly from a double (eq 1) or single (eq 2) exponential fit to the raw data.

Transition State Analysis. The temperature dependence of the binding and dissociation rates was analyzed according to the transition state theory, which relates the rate constant of a reaction to an equilibrium constant between the reactants and the transition state (*26*). The Gibbs free energy of activation ($\Delta G^{\ddagger}$) is related to a rate constant, k, by eq 6:

$$\Delta G^{\ddagger} = -RT \ln \frac{k\hbar}{k_B T} \quad (6)$$

where $\hbar$ is Planck's constant, k_B is the Boltzmann constant, R is the molar gas constant, and T is the temperature. The Gibbs free energy of activation can be separated into its enthalpic ($\Delta H^{\ddagger}$) and entropic ($\Delta S^{\ddagger}$) components by eq 7:

$$\Delta G^{\ddagger} = \Delta H^{\ddagger} - T\Delta S^{\ddagger} \quad (7)$$

Upon rearrangement of eqs 6 and 7, $\Delta H^{\ddagger}$ can be determined from the slope of an Eyring plot, as described by eq 8:

$$\ln \frac{k\hbar}{k_B T} = \frac{-\Delta H^{\ddagger}}{R}\left(\frac{1}{T}\right) + \frac{\Delta S^{\ddagger}}{R} \quad (8)$$

$\Delta S^{\ddagger}$ was calculated from eq 7 using the experimentally derived $\Delta H^{\ddagger}$ and $\Delta G^{\ddagger}$ values.

Isothermal Titration Calorimetry. Thermodynamic parameters were determined at 25 °C using isothermal titration calorimetry (ITC). GST and GS-EA solutions were diluted into a buffer containing 50 mM KPO_4 and 100 mM NaCl, pH 7.0, or 100 mM KPO_4, pH 7.0. GST was dialyzed against the same buffer for 24 h, and all solutions were degassed prior to use. GST (75−200 μM) was titrated with 7−10 μL injections of 1−2 mM GS-EA, and the heat flow between the reaction vessel and an isothermal heat sink was monitored. Nonlinear least-squares fitting of the corrected reaction heat was performed with the Dataworks and Bindworks software, and the dissociation constant (K_d), enthalpy of binding ($\Delta H°$), and stoichiometry of binding (*n)* were determined. The binding data were fit to the equation: $q = nV\Delta H/[\text{EL}]n$, where q is the heat evolved, V is the cell volume, ΔH is the enthalpy change per mole of ligand, [EL] is the concentration of bound ligand, and n is the stoichiometry of binding.

RESULTS

hA1-1 GST Binding and Dissociation Kinetics. Our previous kinetic analyses of ligand binding and dissociation in GST A1-1 have utilized the GST A1-1 from rat, rGST A1-1, due to our extensive series of site-directed mutants within this isoform (*17*, *18*). However, in light of the fact several hGST A1-1 crystal structures have been utilized for comparison to these kinetic data, it is important to directly evaluate the ligand-dependent C-terminal dynamics of hGST A1-1. A stopped-flow binding analysis of wild-type (WT) hGST A1-1 and GS-EA was performed at 20 °C. Rates of GS-EA binding were measured by the decrease in intrinsic protein fluorescence upon mixing 20−400 μM GS-EA with 1 μM hGST A1-1. A representative example of the raw data, fit to a double exponential eq 1, is shown in Figure 2. The rapid relaxation time, k_{obs1}, depended linearly on GS-EA concentration, while the slower relaxation time, k_{obs2}, depended hyperbolically on GS-EA concentration, in agreement with the two-step binding mechanism proposed for WT rGST A1-1 (Scheme 1) (Figure 2, top) (*17*, *18*). According to this two-step mechanism, which includes ligand docking, followed by an isomerization between two [GST·GS-EA]

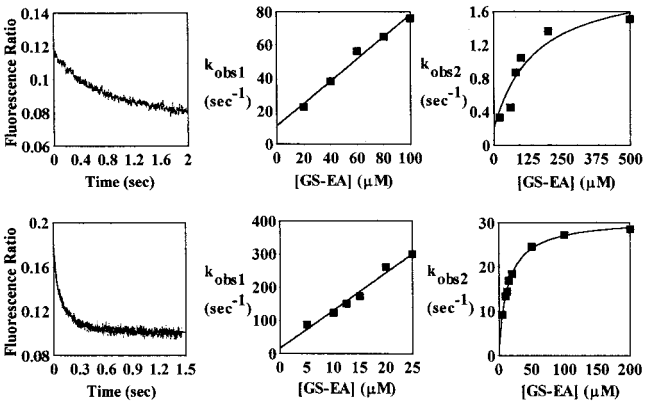

FIGURE 2: Kinetic analysis of GS-EA binding to hGST A1-1 (top) and F222W:W21F rGST A1-1 (bottom). (Top, left) Representative raw data corresponding to the binding of 25 μM GS-EA to 1 μM hGST A1-1. The data fit best to double exponential eq 1 (R^2 = 0.97). (Top, middle) A linear relationship (eq 3) was established between k_{obs1} and [GS-EA] (R^2 = 0.98). (Top, right) A hyperbolic relationship (eq 4) was established between k_{obs2} and [GS-EA] (R^2 = 0.90). (Bottom, left) Representative raw data corresponding to the binding of 50 μM GS-EA to 1 μM F222W:W21F. The data fit best to double exponential eq 1 (R^2 = 0.97). (Bottom, middle) A linear relationship (eq 3) was established between k_{obs1} and [GS-EA] (R^2 = 0.98). (Bottom, right) A hyperbolic relationship (eq 4) was established between k_{obs2} and [GS-EA] (R^2 = 0.99).

Table 1: Kinetic Parameters for GS-EA Binding to WT GST A1-1 and Site-Directed Mutants

	WT[a,b]	F222W:W21F[a]	Δ209−222[a,b]	hGST A1-1[c]
k_{cat} (s^{-1})[d]	2.58	2.42	0.435	
Amp_1[e]	0.0091	0.054	0.0064	0.015
k_1 (μM^{-1} s^{-1})[f,g]	6.11	10.4	3.67	0.67
Amp_{-1}	0.0043	0.037	0.020	0.013
$k_{-1(exp)}$ (s^{-1})[h]	15.9	18.3	23.8	11.5
$k_{-1(calc)}$ (s^{-1})[g]	14.7	16.8	28.5	9.8
K_1 (μM^{-1})[i]	2.60	1.61	6.47	17.2
Amp_2	0.051	0.071		0.035
k_2 (s^{-1})[g]	17.6	21.7		1.8
Amp_{-2}	0.018	0.053		0.055
$k_{-2(exp)}$ (s^{-1})[h]	1.51	2.14		0.22
$k_{-2(calc)}$ (s^{-1})[g]	1.89	2.26		0.21
K_2[i]	0.086	0.099		0.12
K_d (μM^{-1})[j]	0.19	0.117	6.46	1.8

[a] Microscopic kinetic parameters determined at 15 °C. [b] Results obtained from studies in ref (*21*). [c] Microscopic kinetic parameters determined at 20 °C. [d] Steady-state turnover rates with EA at 25 °C. [e] Amplitude values (Amp_1, Amp_{-1}, Amp_2, Amp_{-2}) refer to the magnitude of the preexponential terms for the rate constants, k_1, $k_{-1(exp)}$, k_2, $k_{-2(exp)}$, as determined from stopped-flow experiments. [f] The rate constants for all enzymes were determined from duplicate or triplicate experiments, where 15−30 scans were averaged. The standard deviation was less than ±0.8 for k_1, ±0.7 for k_{-1}, ±0.9 for k_2, and ±0.5 for k_{-2}. [g] Kinetic binding and dissociation constants determined by curve fitting the k_{obs} versus [GS-EA] plots to eqs 3 and 4. [h] Rates of GS-EA dissociation were determined directly from a fit of the raw data to a double (eq 1) or single (eq 2) exponential equation. [i] K_1 is determined from the ratio $k_{-1(exp)}/k_1$; K_2 is determined from the ratio $k_{-2(exp)}/k_2$. [j] Equilibrium dissociation constants were determined from $K_{d(calc)} = K_1 \times [k_{-2}/(k_2 + k_{-2})]$.

complexes, binding and dissociation rates, k_1, $k_{-1(calc)}$, k_2, $k_{-2(calc)}$, were determined (Table 1).

Rates of ligand dissociation were also obtained directly by rapidly mixing 5 mM glutathionesulfonic acid (GSO_3^-) with 2 μM of the [hGST A1-1·GS-EA] complex. Similar to binding reactions, raw data fit best to a double exponential eq 1, yielding $k_{-1(exp)}$ and $k_{-2(exp)}$. The dissociation rates determined directly, $k_{-1(exp)}$ and $k_{-2(exp)}$, agreed well with those determined from the *y*-intercept of the k_{obs} versus [GS-EA] plots, $k_{-1(calc)}$ and $k_{-2(calc)}$ (Figure 2, top).

As discussed previously, the observation of two rate constants for dissociation is unexpected, as the rapid rate, $k_{-1(exp)}$, should be masked by the slower rate, $k_{-2(exp)}$, according to the predicted binding mechanism (*17*). However, the presence of a significant amount of the enzyme in the intermediate complex $[GST{\cdot}ligand]_{dis}$, as estimated by K_2, which presumably does not have a localized C-terminus, supports the observation of two dissociation rates experimentally (Table 1).

These results with hGST A1-1 demonstrate that the binding mechanism is identical to that observed previously in the rat isoform and includes a fast bimolecular reaction, followed by a slow isomerization step (Scheme 1). Notably, k_1 and k_2 are significantly slower for the human isoform, resulting in a lower overall affinity for GS-EA with hGST A1-1 (Table 1).

Binding and Dissociation Kinetics in F222W:W21F rGST A1-1. The binding and dissociation of GS-EA with F222W:W21F, a GST variant where a fluorescent tryptophan has been substituted at the C-terminal residue, was monitored in order to directly probe any conformational changes within the C-terminus during both phases of the binding reaction (Scheme 1). Kinetic studies of ligand binding and dissociation with this double mutant are useful as a comparison to previous results obtained with WT rGST A1-1, which contains Trp-21 as a probe of 'global' changes in protein conformation (Figure 1) (*16, 19*). In principle, the F222W:W21F mutant may reveal additional structural changes which occur upon ligand binding that are localized to the C-terminus. Rates of GS-EA binding were measured by the decrease in intrinsic protein fluorescence upon mixing 20−400 μM GS-EA with 1 μM F222W:W21F rGST A1-1. In binding experiments, a double exponential decay (eq 1) best described the raw data from 5 to 15 °C, yielding k_{obs1} and k_{obs2} (Figure 2, bottom). These observed rates were linearly and hyperbolically dependent upon GS-EA concentration, similar to our results with WT rGST A1-1 from 10 to 20 °C and hGST A1-1 at 20 °C (Scheme 1 and Figure 2, bottom) (*17*).

In contrast, raw data corresponding to ligand binding to F222W:W21F from 20 to 40 °C fit best to a single exponential decay (eq 2). The rapid step of the binding reaction has apparently become too fast to measure, as these observed rates were also hyperbolically dependent on GS-EA concentration (data not shown) (*17, 18*). These rates, k_2 and $k_{-2(calc)}$, as well as the equilibrium constant governing the first step of the binding reaction, K_1, were determined by curve-fitting to eq 5.

Rates of ligand dissociation were obtained directly by the rapid mixing of 5 mM glutathionesulfonic acid (GSO_3^-) with 2 μM of the [F222W:W21F·GS-EA] complex. The raw data describing the dissociation reaction fit best to double exponential eq 1 for F222W:W21F at temperatures up to 40 °C, yielding $k_{-1(exp)}$ and $k_{-2(exp)}$ (Table 2). As discussed with hGST A1-1, the observation of two relaxation times for the dissociation reaction is due to a significant portion of the intermediate precomplex $[GST{\cdot}ligand]_{dis}$ at equilibrium (K_2 = 0.099).

Table 2: Thermodynamic Parameters Governing GS-EA Binding to WT, Δ209−222, and F222W:W21F rGST A1-1

	WT	Δ209−222	F222W:W21F
$\Delta H_1°$ (kcal/mol)[a]	9.53	−9.26	9.1
$\Delta G_1°$ (kcal/mol)[a]	−7.37	−6.62	−7.65
$\Delta S_1°$ [cal/(mol·K)][a]	58.7	−10.8	58.1
$\Delta H_2°$ (kcal/mol)[b]	−15.2	*c*	−13.0
$\Delta G_2°$ (kcal/mol)[b]	−1.4		−1.5
$\Delta S_2°$ [cal/(mol·K)][b]	−47.9		−40.1
$\Delta H_{tot}°$ (kcal/mol)[d]	−5.67	−9.26	−3.9
$\Delta G_{tot}°$ (kcal/mol)[d]	−8.77	−6.62	−9.15
$\Delta S_{tot}°$ [cal/(mol·K)][d]	10.8	−10.8	18.0
$\Delta H°$ (kcal/mol)[e]	−7.60	−14.8	ND[f]
$\Delta G°$ (kcal/mol)[e]	−9.34	−8.01	
$\Delta S°$ [cal/(mol·K)][e]	5.84	−23.3	
n[g]	2.12	2.06	

[a] Calculated from $\Delta H_1° = \Delta H_1^{‡} - \Delta H_{-1}^{‡}$, $\Delta G_1° = \Delta G_1^{‡} - \Delta G_{-1}^{‡}$, $\Delta S_1° = \Delta S_1^{‡} - \Delta S_{-1}^{‡}$. [b] Calculated from $\Delta H_1° = \Delta H_1^{‡} - \Delta H_{-1}^{‡}$, $\Delta G_1° = \Delta G_1^{‡} - \Delta G_{-1}^{‡}$, $\Delta S_1° = \Delta S_1^{‡} - \Delta S_{-1}^{‡}$. [c] A second relaxation time was not observed during ligand binding and dissociation experiments with Δ209−222. [d] Calculated from $\Delta H_{tot}° = \Delta H_1° + \Delta H_2°$, $\Delta G_{tot}° = \Delta G_1° + \Delta G_2°$, $\Delta S_{tot}° = \Delta S_1° + \Delta S_2°$. [e] Determined from ITC experiments at 25 °C. [f] Not determined. [g] The stoichiometry of ligand binding per GST dimer, as determined by ITC.

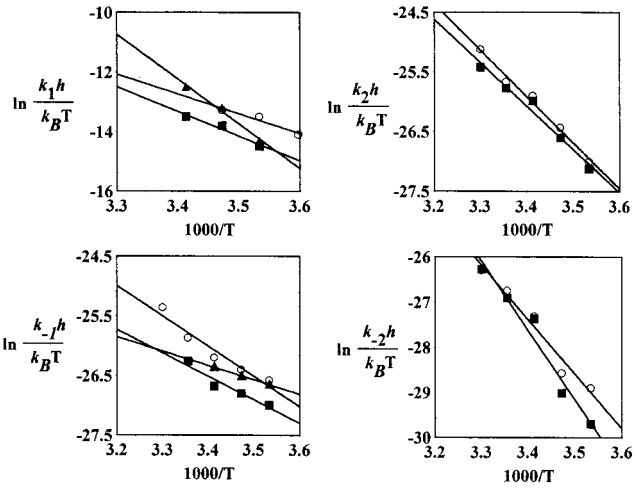

FIGURE 3: Dependence of the binding and dissociation rates on temperature. (Left) Eyring plot for the ligand docking steps of the binding reaction, k_1 (top) and k_{-1} (bottom), for WT (solid squares), F222W:W21F (open circles), and Δ209−222 (solid triangles). (Right) Eyring plot for the isomerization steps of the binding reaction, k_2 (top) and k_{-2} (bottom). $\Delta H^{‡}$ values were determined by curve fitting to eq 8. All R^2 values were above 0.95.

Because the fluorescent probe in the F222W:W21F variant is the C-terminal residue, the observation of a two-step mechanism of ligand binding demonstrates that the environment of Trp-222 changes during both ligand docking (k_1) and isomerization (k_2). Although a conformational change within the C-terminus during the isomerization phase had been clear from our previous results with WT and Δ209−222, the F222W probe provides additional evidence that the C-terminus of GST A1-1 contributes to the ligand docking step (k_1 and k_{-1}) of the binding reaction, as well as the isomerization (k_2 and k_{-2}) (*17*).

Thermodynamic Binding Parameters in Δ209−222, WT, and F222W:W21F rGST A1-1. To elucidate how the C-terminus affects the thermodynamics of ligand binding, we monitored the temperature dependence of binding and dissociation to WT, F222W:W21F, and Δ209−222 rGST A1-1. Eyring plots were linear to 40 °C for each enzyme, suggesting that there are no significant changes in protein conformation or in the binding mechanism from 10 to 40 °C (Figure 3) (*27*). The enthalpy of activation for each phase of the binding reaction, $\Delta H^{‡}_1$, $\Delta H^{‡}_{-1}$, $\Delta H^{‡}_2$, $\Delta H^{‡}_{-2}$, was determined from the slope of the Eyring plot, according to eq 8. The entropies ($\Delta S^{‡}$) and free energies ($\Delta G^{‡}$) of activation were determined from eqs 6 and 7, respectively. These activation parameters were used to calculate the thermodynamic binding parameters in Table 2.

The thermodynamic parameters provide a clear distinction between ligand binding to WT or F222W:W21F rGST A1-1 versus a C-terminal truncation mutant, Δ209−222. During ligand docking, the favorable contribution to $\Delta G_1°$ in WT and F222W:W21F, where $\Delta G_1° = \Delta G_1^{‡} - \Delta G_{-1}^{‡}$, is entropic [58.7 and 58.1 cal/(mol·K), respectively], and the reaction is unfavorable enthalpically. In contrast, the opposite is true in Δ209−222; ligand docking is completely enthalpically driven (−9.26 kcal/mol) and entropically unfavorable (Table 2). Highly favorable binding entropy and unfavorable enthalpy are characteristic for the displacement of water from the contact interface (*28*). The entropy gain is attributed to desolvation of nonpolar groups and release of ordered water into bulk solvent upon binding, while the unfavorable enthalpy is due to the burial of hydrophobic groups. In WT and F222W:W21F, the active site desolvation, which apparently overcomes the entropic loss in ligand or protein flexibility upon complexation of the two moieties (GST and GS-EA) during k_1, is not surprising. X-ray crystal structures clearly illustrate that the active site of ligand-bound hA1-1 contains fewer structured water molecules than the apoenzyme (*13*, *14*). However, the involvement of the C-terminus in this desolvation event within the *first* phase of the binding reaction, as illustrated by comparison of the $\Delta S_1°$ values for WT and Δ209−222, is quite striking (Table 2).

As expected for a protein containing a flexible segment, enthalpic interactions are maximized during the second step of the binding reaction in WT or F222W:W21F (*29*, *30*). During this step of the reaction, the flexible residues presumably 'mold' to the specific ligand, thereby forming the van der Waals or hydrogen bonding interactions which stabilize the localized helix. The unfavorable entropy observed during the isomerization phase in WT or F222W:W21F demonstrates that this step is not coupled to desolvation.

As an independent approach, isothermal titration calorimetry (ITC) was used to determine the thermodynamic parameters which govern ligand binding. In ITC, the heat flux which occurs during ligand binding is measured directly. Therefore, all of the binding parameters, $\Delta H°$, $\Delta G°$, and the stoichiometry of binding, *n*, can be detected within a single experiment. However, ITC cannot resolve the thermodynamic parameters for the individual steps within the binding reaction. Therefore, the recovered parameters reflect the changes for the weighted average transition from [GST] to $[GST·ligand]_{dis}$ and $[GST·ligand]_{ord}$. Nevertheless, the thermodynamic binding parameters governing GS-EA binding to WT and Δ209−222 rGST A1-1 determined by ITC were consistent with the kinetically determined parameters (Figure 4 and Table 2). Overall, ligand binding to WT or F222W:W21F is driven by a combination of entropy (from k_1) and enthalpy (from k_2), while binding to Δ209−222 is enthal-

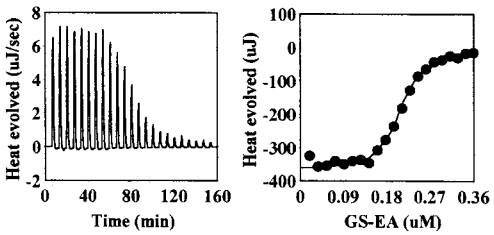

FIGURE 4: (Left) Raw data for a representative isothermal calorimetric titration curve of WT rGST A1-1 and GS-EA. The cell contained 150 μM WT rGST A1-1. 10 μL injections of 1.5 mM GS-EA were made at 300 s intervals. (Right) Curve fit of the data, yielding the parameters in Table 2. The stoichiometry of binding for GS-EA recovered from the ITC data is 2.06 and 2.12 ligands/dimer for the WT and Δ209−222, respectively.

pically driven (Table 2). Additionally, the stoichiometry of ligand binding, *n*, confirmed that two GS-EA ligands bind per GST dimer in each protein, consistent with our previous results with the WT enzyme (*18*). When the ITC data were analyzed using a value for the concentration of protein equal to the dimer, the recovered stoichiometry was 2 per dimer (Table 2). When the same data were analyzed using a value for the concentration of protein equal to the monomeric subunits, the recovered stoichiometry values were 1 per subunit. Notably, no evidence for ligand binding cooperativity was observed with ITC. Because the available X-ray structure of [GSTA1-1·GS-EA] cannot unambiguously determine the binding stoichiometry, the ITC experiments provide essential confirmation that each subunit binds GS-EA. This further supports the model wherein the kinetic phases correspond to two steps of a reaction that occurs on each subunit.

DISCUSSION

According to transition state theory, analysis of the temperature dependence of a kinetic process allows for the determination of the activation parameters describing the differences between a ground state and the transition state of a binding reaction. In principle, knowledge of these differences may provide information about the reaction mechanism. Here, we performed a kinetic and thermodynamic analysis of GST A1-1 to gain insight into the nature of the binding forces that drive ligand binding and the corresponding C-terminal structural transition. Although there has been considerable interest in the C-terminus and its role in catalysis, in ligand function, and in ligand dissociation and binding, an exhaustive thermodynamic analysis describing ligand binding to any of the GSTs has not been performed (*16*−*18*, *31*−*34*).

We recently demonstrated that binding of a glutathione product conjugate to rGST A1-1 proceeds via a two-step mechanism, including ligand docking (k_1), followed by an isomerization between two complexes, $[GST{\cdot}ligand]_{dis}$ and $[GST{\cdot}ligand]_{ord}$ (Scheme 1) (*17*, *18*). The isomerization clearly involves the C-terminus, since the relaxation time corresponding to this step of the binding mechanism was not observed in a C-terminal truncation mutant, Δ209−222 (*17*). To confirm that a multistep binding mechanism is not unique to the GST A1-1 isoform from rat, we monitored ligand binding and dissociation to hGST A1-1, the human GST A1-1. Consistent with our previous results, the two relaxation times which best described the raw data in hGST A1-1 were linearly dependent and hyperbolically dependent upon GS-EA concentration (Figure 2) (*17*). Apparently, the mechanism of ligand binding in the two GST isoforms, rGST A1-1 and hGST A1-1, is nearly identical. Surprisingly, however, rates of ligand binding, k_1 and k_2, and to a lesser extent dissociation, k_{-1} and k_{-2}, were much slower in human versus rat GST A1-1 (Table 1). Further studies will have to be performed to explain the basis of these isoform-dependent differences.

In WT rGST A1-1, the residue that primarily contributes to changes in intrinsic protein fluorescence during ligand binding is Trp-21, the single tryptophan within each monomer (*16*, *19*). The available crystal structures indicate that upon binding of a glutathione conjugate, there is a subtle change at the domain−domain interface, which includes the α-1 helix, containing Trp-21. This helix pivots slightly upon ligand binding, resulting in a slight change in the environment of Trp-21. Therefore, this residue is a probe of 'global' changes within the protein during ligand binding. To directly monitor local conformational changes within the C-terminus, we substituted a tryptophan at the C-terminal residue, 222, and a spectroscopically 'invisible' phenylalanine at position 21 (Figure 1). Enzymatic activity with the F222W:W21F rGST A1-1 protein is comparable to WT rGST A1-1, indicating that the double mutant is structurally and dynamically intact.

A reviewer suggested that the observed biphasic kinetics at the high GS-EA:GST ratios used in our studies could be due to two separate classes of binding sites, with different ligand affinities. In principle, the hydrophobic portion of GS-EA could bind, presumably with lower affinity, to a site other than the hydrophobic substrate binding site. In this case, the binding mechanism would include parallel reversible pathways, rather than the sequential steps in Scheme 1. If the affinities for the two sites were sufficiently different, then the observed relaxation could collapse to a single rate at stoichiometric GS-EA:GST ratios. We have performed kinetic simulations with protein concentrations used in our experiments (2 μM) and with on and off rates corresponding to our observed rate constants. We have performed simulations with an excess of ligand (20 μM) and at stoichiometric ligand concentrations (2 μM). The simulations indicate that upon reducing the ligand concentration from 20 to 2 μM the observed kinetics change from a biphasic relaxation process to a monophasic relaxation. We have, therefore, examined experimentally the kinetics of binding at a 1:1 GS-EA:GST ratio. At this stoichiometric ratio, biphasic kinetics are observed. A 'best fit' of the relaxation data at this concentration of ligand fits poorly to a fast component that is clearly present in the raw data (not shown). Upon fitting these data to two relaxation times, the recovered k_{obs} values are well-resolved and differ by a factor of 9.4. The sequential mechanism, with two steps occurring at a single class of sites, also is supported by results with several mutants. We have observed that the conservative mutation at the active site, Y9F, significantly alters both relaxation times for binding of a smaller, less hydrophobic GSH conjugate (*18*). It is unlikely that such a conservative mutation at the active site would affect the kinetics of binding to a separate site. Moreover, we have examined the kinetics of binding for several mutants with substitutions at Phe-10, which directly contacts Tyr-9 in the apo GSTA1-1. Mutations at Phe-10

also affect both of the observed relaxation times (unpublished data). Again, it is unlikely that mutations within a localized region would have such large effects on both relaxation times, if one of the kinetic phases corresponded to binding at a remote site. Also, our previous work (*17*) and the current work demonstrate that the C-terminus is a critical determinant of the second slow phase, but has little impact on the first phase. It is difficult to reconcile how the C-terminus could be important specifically in the second phase and Phe-10 could markedly affect the first phase, if the phases corresponded to binding at separate sites. Because the available structural data indicate that interactions between Tyr-9, Phe-10, and the C-terminus determine the dynamics of the C-terminus, it would be expected that mutations at these residues would alter binding kinetics at the active site. Finally, in all of the literature concerning X-ray structures of GSTA1-1 complexed with GSH conjugates, including the ligand used here, no additional binding sites have been observed or suspected. Taken together, the available data are most consistent with a sequential two-step (or more) binding mechanism at the active site.

The two-step binding mechanism which describes ligand binding to F222W:W21F illustrates that the environment of Trp-222 is altered during both ligand docking (k_1) and the isomerization (k_2) (Scheme 1). In conjunction with fluorescence experiments and X-ray crystal structures, which suggest that the C-terminus exists in a number of conformations that are dependent upon the bound ligand, these results provide evidence for an intermediate conformation of the C-terminus in $[GST{\cdot}ligand]_{dis}$, which is distinct from the apoenzyme and the localized, crystallographically observable helical conformation *(15, 16, 33, 34)*.

Surprisingly, however, rates of GS-EA binding and dissociation in F222W:W21F do not significantly differ from the WT enzyme (Table 1). Apparently, the changes at the domain−domain interface, which cause the fluorescence quenching of Trp-21 in WT, occur on the same time-scale as the local changes in the 14-residue C-terminal segment in F222W:W21F. Furthermore, the equilibrium constants, K_2, for the transition between $[GST{\cdot}ligand]_{dis}$ and $[GST{\cdot}ligand]_{ord}$ are similar in WT and F222W:W21F, suggesting that the mutations do not alter the equilibrium between the two complexes, even with a bulkier indole side chain at the C-terminal residue in F222W:W21F (Table 1).

Flexible segments within proteins commonly enhance the enthalpy of binding interactions, due to their ability to adapt to a particular ligand. As illustrated in binding experiments with Cdc42Hs, a GTP-binding protein, and hemopoietic cell kinase, conformational flexibility within the C-terminus, allows each protein to maximize enthalpy at the protein−ligand interface (*29, 30*). To elucidate the thermodynamic forces that drive ligand binding and the corresponding C-terminal transition in rGST A1-1, activation parameters were determined by monitoring the temperature dependence of each step of the binding and dissociation reaction to WT, F222W:W21F, and the C-terminal truncation mutant, Δ209−222 (Table 2). Net changes in entropy and enthalpy are a sum of contributions from hydration effects, polar interactions (hydrogen bonding and ion pairs), and nonpolar interactions (van der Waals contacts). The hydration effects which contribute to $\Delta S°$ involve a balance between changes in the degree of hydration of the enzyme and ligand upon binding, the loss of translational and rotational degrees of freedom upon formation of the complex, and changes in rotational and vibrational entropy due to the loss of conformational flexibility in the enzyme and ligand. In general, contributions to $\Delta H°$ reflect the formation or removal of hydrogen bonds, van der Waals forces, and electrostatic interactions between the protein, ligand, and solvent molecules.

Scheme 2

$$\text{Ligand} + \text{GST} \underset{k_{-1}}{\overset{k_1}{\rightleftharpoons}} [GST{\cdot}Ligand]_{dis} \underset{k_{-2}}{\overset{k_2}{\rightleftharpoons}} [GST{\cdot}Ligand]_{ord}$$

Desolvation
Entropically-driven

Tertiary Packing of the C-terminus
Enthalpically-driven

A combination of entropic and enthalpic forces drives ligand binding within WT rGST A1-1. However, there is a dramatic difference in the contribution of entropy or enthalpy to the individual steps of the binding reaction. An entropically favorable and enthalpically unfavorable ligand docking step (k_1) suggests that the active site and C-terminus are highly solvated in the apoenzyme (*28*). The displacement of structured water and the burial of hydrophobic groups upon ligand docking apparently overcome the negative entropy resulting from losses of translational, rotational, and vibrational degrees of freedom upon complexation of the enzyme and ligand. The second step of the binding reaction, the transition of the C-terminal helix to its localized, well-packed position over the active site, comprises the favorable enthalpic component of binding energy in WT and is entropically unfavorable. Comparison of the thermodynamic parameters in F222W:W21F to those in WT indicates that the double mutation does not alter the forces which drive ligand binding. However, comparisons of the WT or F222W:W21F thermodynamic parameters with Δ209−222 demonstrate the most surprising results of our study: the C-terminus is required for the favorable entropic contribution to binding, and desolvation precedes the transition of the C-terminus to its final localized state. These results are summarized schematically in Scheme 2.

These thermodynamic results may have several physiological implications regarding the role of the C-terminus in GST A1-1 catalysis. Steady-state turnover rates with cumene hydroperoxide (CHP) and CDNB, for which chemical steps are at least partially rate-limiting, are increased (>100-fold) in WT versus a C-terminal truncation mutant (*21, 31, 34*). Therefore, the C-terminus clearly contributes to the chemical step of the reaction. Additionally, our kinetic and thermodynamic studies demonstrate that the structural transition of the C-terminus to an intermediate conformation in $[GST{\cdot}ligand]_{dis}$ contributes to the active site desolvation which drives ligand docking within the binding mechanism. These two observations suggest that the contribution of the C-terminus to substrate turnover in GST A1-1 may be due, in part, to the active site desolvation that occurs upon binding of the hydrophobic substrate. The importance of active site desolvation to GST catalysis and, specifically, to formation of the nucleophilic thiolate within the ternary complex, [GST·GSH·substrate], has been discussed previously (*35, 36*). Our thermodynamic results support these studies and directly demonstrate that the active site desolvation, which is critical to ligand docking in GST A1-1, is due to the C-terminus. Therefore, turnover rates for substrates which are rate-limited

by the chemical step of the reaction may be significantly reduced in a C-terminal truncation mutant, in part because this desolvation does not occur in the absence of the C-terminus. Even more importantly, if desolvation is the 'catalytic' contribution provided by the C-terminus, the intermediate state, $[GST{\cdot}ligand]_{dis}$, is catalytically active, and a localized, 'closed' C-terminal helix, $[GST{\cdot}ligand]_{ord}$, is not required for substrate turnover.

Our results provide several new insights into the kinetic and thermodynamic role of the C-terminus in GST A1-1 catalysis. The two-step binding mechanism, which includes ligand docking (k_1), followed by a conformation change of the C-terminus (k_2), is appropriate for hGST A1-1, confirming the binding mechanism proposed for rGST A1-1. Our results with F222W:W21F extend this mechanism further and provide evidence that the C-terminus has an intermediate conformation in $[GST{\cdot}ligand]_{dis}$, which is distinct from either the apoenzyme or the localized, well-packed helix in $[GST{\cdot}ligand]_{ord}$. However, the most striking result of these studies to GST A1-1 catalysis is that the C-terminus is required for an entropically driven ligand docking step, which precedes isomerization of the C-terminus to its final state. These results suggest that the C-terminus contributes to GST A1-1 catalysis by desolvation.

Finally, it is useful to compare the present model for binding and dissociation of GSH conjugates with the binding of GSH to GSTA1-1, as described by Gustafsson et al. (*34*), and to GSTM1-1, as elucidated by Parsons et al. (*37*). For both isoforms, a single relaxation rate was observed for the approach to equilibrium upon binding GSH. Because the observed rate constants for both isoforms were well below the diffusion-controlled limit, both groups invoked a fast preequilibrium of enzyme conformers, wherein GSH binding occurred selectively with one conformation. The available X-ray structure of the apo GSTA1-1 clearly suggests the existence of multiple conformations in the absence of ligand, and the fast preequilibrium between these conformations is an implicit component of our model. Certainly, the initial docking of GSH conjugates (k_1/k_{-1} in our model) occurs with preference for some conformers. Thus, the binding model for GSH described by Gustafsson et al. is not inconsistent with our model for binding of GSH conjugates. The lack of a slow isomerization (k_2/k_{-2} of our model) with GSH binding (*34*) merely underscores the inability of GSH to drive the C-terminus to the 'closed' conformation, as suggested by the X-ray structure of $[rGSTA1\text{-}1{\cdot}GSO_3^-]$ (*15*). Because the equilibria between multiple conformations of the C-terminus within the apo enzyme are kinetically unresolved in our experiments, we have not explicitly included them in our model. Rapidly equilibrating conformers are 'lumped into' a single state.

REFERENCES

1. Mannervik, B., Ålin, P., Guthenberg, C., Jensson, H., Tahir, M. K., Warholm, M., and Jörnvall, H. (1985) *Proc. Natl. Acad. Sci. U.S.A. 82,* 7202−7206.
2. Meyer, D. J., Coles, B., Pemble, S. E., Gilmore, K. S., Fraser, G. M., and Ketterer, B. (1991) *Biochem. J. 274,* 409−414.
3. Pemble, S. E., Wardle, A. F., and Taylor, J. B. (1996) *Biochem. J. 319,* 749−754.
4. Meyer, D. J., and Thomas, M. (1995) *Biochem. J. 311,* 739−742.
5. Board, P. G., Baker, R. T., Chelvanayagam, G., and Jermiin, L. S. (1997) *Biochem. J. 328,* 929−935.
6. Kong, K. H., Takasu, K., Inoue, H., and Takahashi, K. (1992) *Biochem. Biophys. Res. Commun. 184,* 194−197.
7. Liu, S., Zhang, P., Ji, X., Johnson, W. W., Gilliland, G. L., and Armstrong, R. N. (1992) *J. Biol. Chem. 267,* 4296−4299.
8. Huskey, S. E., Huskey, W. P., and Lu, A. Y. H. (1991) *J. Am. Chem. Soc. 113,* 2283−2290.
9. Liu, S., Ki, X., Gilliland, G. L., Stevens, W. J., and Armstrong, R. N. (1993) *J. Am. Chem. Soc. 115,* 7910−7911.
10. Wang, R. W., Newton, D. J., Huskey, S. E. W., McKeever, B. M., Pickett, C. B., and Lu, A. Y. H. (1992) *J. Biol. Chem. 267,* 19866−19871.
11. Armstrong, R. N. (1991) *Chem. Res. Toxicol. 4,* 131−139.
12. Armstrong, R. N. (1997) *Chem. Res. Toxicol. 7,* 1−10.
13. Cameron, A., Sinning, I., L'Hermite, G., Olin, B., Board, P. G., Mannervik, B., and Jones, A. (1995) *Structure 3,* 717−727.
14. Sinning, I., Kleywegt, G., Cowan, S., Reinemer, P., Dirr, H., Huoer, R., Gilliland, G., Armstrong, R. N., Ji, X., Board, P. G., Olin, B., Mannervik, B., and Jones, T. (1993) *J. Mol. Biol. 232,* 192−212.
15. Adman, E. T., Le Trong, I., Stenkamp, R. E., Nieslanik, B. S., Dietze, E. C., Tai, G., Ibarra, C., and Atkins, W. M. (2001) *Proteins: Struct., Funct., Genet.* (in press).
16. Dirr, H. W., and Wallace, L. A. (1999) *Biochemistry 38,* 5631−5640.
17. Nieslanik, B. S., Dabrowski, M. J., Lyon, R. P., and Atkins, W. M. (1999) *Biochemistry 38,* 6971−6980.
18. Nieslanik, B. S., and Atkins, W. M. (2000) *J. Biol. Chem. 275,* 17447−17451.
19. Wang, R. W., Bird, A. W., Newton, D. J., Lu, A. Y. H., and Atkins, W. M. (1993) *Protein Sci. 2,* 2085−2094.
20. Nieslanik, B. S., and Atkins, W. M. (1998) *J. Am. Chem. Soc. 120,* 6651−6660.
21. Widersten, M., Bjornstedt, R., and Mannervik, B. (1996) *Biochemistry 35,* 7731−7742.
22. Ploeman, J. H. T. M., Van Ommen, B., Bogards, J. J. P., and Van Bladeren, P. J. (1990) *Biochem. Pharmacol. 40,* 1631−1635.
23. Dietze, E. C., Wang, R. W., Lu, A. Y. H., and Atkins, W. M. (1996) *Biochemistry 35,* 6745−6753.
24. Wang, R. W., Pickett, C. B., and Lu, A. Y. H. (1989) *Arch. Biochem. Biophys. 269,* 536−543.
25. Habig, W., Pabst, M., and Jakoby, W. (1974) *J. Biol. Chem. 249,* 7139−7140.
26. Fersht, A. (1999) *Structure and Mechanism in Protein Science,* pp 54−58, 132−158, W. H. Freeman & Co., New York.
27. Segel, I. H. (1975) *Enzyme Kinetics: Behavior and analysis of rapid equilibrium and steady-state enzyme systems,* pp 934−938, John Wiley & Sons, New York.
28. Velazquez-Campoy, A., Todd, M. J., and Freire, E. (2000) *Biochemistry 39,* 2201−2207.
29. Arold, S., O'Brien, R., Franken, P., Strub, M.-P., Hoh, F., Dumas, C., and Ladbury, J. E. (1998) *Biochemistry 37,* 14683−14691.
30. Loh, A. P., Guo, W., Nicholson, L. K., and Oswald, R. E. (1999) *Biochemistry 38,* 12547−12557.
31. Board, P. G., and Mannervik, B (1991) *Biochem. J. 275,* 171−174.
32. Atkins, W. M., Dietze, E. C., and Ibarra, C. (1997) *Protein Sci. 6,* 873−881.
33. Gustafsson, A., Etahadieh, M., Jemth, P., and Mannervik, B. (1999) *Biochemistry 38,* 16268−16275.
34. Allardyce, C. S., McDonagh, P. D., Lian, L. Y., Wolf, C. R., and Roberts, G. C. (1999) *Biochem. J. 343,* 525−531.
35. Huskey, S.-E. W., Huskey, W. P., and Lu, A. Y. H. (1991) *J. Am. Chem. Soc. 113,* 2283−2290.
36. Xiao, G., Liu, S., Ji, X., Johnson, W. W., Chen, J., Parsons, J. F., Stevens, W. J., Gilliland, G. L., and Armstrong, R. N. (1996) *Biochemistry 35,* 4753−4765.
37. Parsons, J. F., Xiao, G., Gilliland, G. L., and Armstrong, R. N. (1998) *Biochemistry 37,* 6286−6294.

BI001869X